Received: 16 June 2019 | Revised: 6 November 2019 | Accepted: 29 November 2019

DOI: 10.1111/jnc.14933

ORIGINAL ARTICLE

Journal of Neurochemistry JNC The Official Journal of the International Society for Neurochemistry WILEY

The constitutive activity of melanocortin-4 receptors in cAMP pathway is allosterically modulated by zinc and copper ions

Reet Link[1] | Santa Veiksina[1] | Maris-Johanna Tahk[1] | Tõnis Laasfeld[1] | Päärn Paiste[2] | Sergei Kopanchuk[1] | Ago Rinken[1]

[1]Institute of Chemistry, University of Tartu, Tartu, Estonia

[2]Department of Geology, University of Tartu, Tartu, Estonia

Correspondence
Ago Rinken and Sergei Kopanchuk, Institute of Chemistry, University of Tartu, Ravila 14a, 50411 Tartu, Estonia
Email: ago.rinken@ut.ee (A. R.) and
Email: sergei.kopanchuk@ut.ee (S. K.)

Funding information
Estonian Research Council, Grant/Award Number: IUT20-17 and PSG230

Abstract

Melanocortin-4 receptors (MC_4R) are unique among G-protein-coupled receptors (GPCRs) as they have endogenous ligands that can exhibit inverse agonistic properties in the case of elevated basal activity. It is known that the constitutive activity of GPCRs strongly affects the ligand-dependent physiological responses, but little is known about these regulatory mechanisms. Since several metal ions have been shown to be important modulators of the signal transduction of GPCRs, we hypothesized that metal ions regulate the basal activity of MC_4Rs. Implementation of a fluorescence anisotropy assay and novel redshifted fluorescent peptides enabled kinetic characterization of ligand binding to MC_4R expressed on budded baculoviruses. We show that Ca^{2+} is required for high-affinity ligand binding, but Zn^{2+} and Cu^{2+} in the presence of Ca^{2+} behave as negative allosteric modulators of ligand binding to MC_4R. FRET-based cAMP biosensor was used to measure the activation of MC_4R stably expressed in CHO-K1 cells. At low micromolar concentrations, Zn^{2+} caused MC_4R-dependent activation of the cAMP pathway, whereas Cu^{2+} reduced the activity of MC_4R even below the basal level. These findings indicate that at physiologically relevant concentrations can Zn^{2+} and Cu^{2+} function as MC_4R agonists or inverse agonists, respectively. This means that depending on the level of constitutive activity induced by Zn^{2+} ions, the pharmacological effect of orthosteric ligands of MC_4R can be switched from a partial to an inverse agonist.

KEYWORDS

constitutive activity, copper, G protein-coupled receptor (GPCR), inverse agonism, melanocortin-4 receptor (MC_4R), zinc

1 | INTRODUCTION

The important role of melanocortin-4 receptors (MC_4R) in energy homeostasis, sexual functions, neuroprotection, and neurogenesis (Wikberg and Mutulis, 2008; Tao, 2010) has made these G protein-coupled receptors attractive drug targets in the central nervous system (CNS). Despite being very promising targets for several clinical trials, there is only a limited number of therapeutically approved drugs for MC_4Rs (Ericson *et al.*, 2017), mainly because the signal transduction of MC_4Rs is subject to considerable complexity including conformational adjustments, oligomerization, and effects of different modulators (Biebermann *et al.*, 2003; Kopanchuk *et al.*,

Abbreviations used: AgRP, agouti-related protein; BacMam, baculovirus gene transfer into mammalian cells; BBV, budded baculoviruses; CHO-K1, chinese hamster ovary cells; CNS, central nervous system; FA, fluorescence anisotropy; G proteins, guanine nucleotide-binding proteins; GPCR, G-protein-coupled receptor; ICP-MS, inductively coupled plasma mass spectrometry; MC_1R, melanocortin-1 receptor; MC_4R, melanocortin-4 receptor; MOI, multiplicity of infection; RRID, Research Resource Identifier; Sf9, spodoptera frugiperda cells.

2005; Müller, Berkmann, Scheerer, Biebermann, and Kleinau, 2016). There is increasing evidence that MC_4R can form homo- and heterodimers or higher-order oligomers (Elsner *et al*., 2006; Kopanchuk *et al*., 2006; Nickolls and Maki, 2006; Rediger *et al*., 2009; Chapman and Findlay, 2013) and the ligand binding within MC_4R homodimers is governed by asymmetric regulation of co-operative-binding sites (Kopanchuk *et al*., 2006, 2005). Recently, this has also been confirmed with functional studies (Lensing *et al*., 2019).

The complexity of the MC_4R system is also connected with its high constitutive activity, that is, agonist-independent signaling, and signaling bias involving different response pathways (Tao, 2014; Yang and Tao, 2017). The level of GPCR basal activity plays a critical role in determining the ligand-binding properties and signaling spectrum of the receptors (Kenakin, 2005b; Bond and IJzerman 2006). In the case of MC_4R, the endogenous and synthetic antagonists have shown to behave as inverse agonists or partial agonists in cAMP pathway, depending on the level of constitutive activity (Haskell-Luevano and Monck, 2001; Nijenhuis, Oosterom, and Adan, 2001; Lensing *et al*., 2019). Some naturally occurring mutations in MC_4R can cause either loss or increase in constitutive activity potentially leading to pathogenesis of obesity or anorexia nervosa, respectively (Tao, 2014). Despite the importance of GPCRs' ability to exhibit basal activity, the underlying regulatory mechanism has not yet been clearly established.

It has been shown that different metal ions can diversely modulate the signaling of numerous GPCRs by changing ligand-binding properties or efficacies to transduce signals (May, Leach, Sexton, and Christopoulos, 2007; Westhuizen, Valant, Sexton, and Christopoulos, 2015). In the case of the melanocortin receptors, Ca^{2+} has been found to be essential for high-affinity ligand binding and efficient signal transduction (Kopanchuk *et al*., 2005; Veiksina, Kopanchuk, and Rinken, 2010; Mazina, Reinart-Okugbeni, Kopanchuk, and Rinken, 2012). Zn^{2+} and Cu^{2+} have been found to inhibit ligand binding to MC_4R (Holst, Elling, and Schwartz, 2002; Lagerström *et al*., 2003), whereas their influence on signal transduction has remained inconsistent. Holst *et al*. (2002) found that Zn^{2+} behaved as an agonist of MC_4R and enhanced the action of MC_4R peptide agonist whereas Lagerström *et al*. (2003) found that Zn^{2+} exhibited no agonistic behavior itself and inhibited the action of MC_4R peptide agonist. The inconsistencies may be because of the kinetic characteristics of the ligands, and this aspect has therefore received greater attention in this work.

The kinetic studies of ligand binding to GPCRs have become considerably easier after the implementation of novel fluorescence-based methods, which allow the monitoring of the process in real-time without the need to separate free and bound ligands (Hoffmann *et al*., 2015). A fluorescence anisotropy (FA)-based assay has been successfully applied in kinetic studies of ligand binding to MC_4R (Veiksina *et al*., 2010). The homogeneity of this assay system, which is important for kinetic studies, is improved by the implementation of budded baculoviruses (BBV) as the source of receptors (Rinken, Lavogina, and Kopanchuk, 2018). The kinetic rate constants of ligand binding have been determined using the fluorescently labeled peptide NDP-α-MSH (Veiksina *et al*., 2010), but the reaction equilibrium is not reached because of slow dissociation of the MC_4R-fluorescent ligand complex. Therefore, two novel redshifted peptides with faster kinetics have been implemented to resolve a broader range of modulatory effects (Link, Veiksina, Rinken, and Kopanchuk, 2017). The FRET-based biosensors have opened up novel possibilities also for monitoring the activation of signal transduction pathways in real-time (Unen *et al*., 2015). Thus, the kinetic data can be obtained for both ligand binding as well as signal transduction processes.

In the current work, we used FA-based ligand binding (Veiksina *et al*., 2015) and FRET-based functional assays of the cAMP pathway (Mazina, Allikalt, *et al*., 2015a) to study the effects of several divalent metal ions on the MC_4R. Studying the metal ion effects from a ligand binding and functional perspective is especially important in the case of an allosteric modulation mechanism, where a negative modulator of the ligand binding may be a positive modulator of the signal transduction or vice versa. We observed this phenomenon for Zn^{2+} and Cu^{2+} ions, which are both negative allosteric modulators of ligand binding, but Zn^{2+} acts as an activator and Cu^{2+} as an inhibitor of the basal activity of MC_4R in cAMP pathway. These findings could be physiologically relevant, as zinc and copper are required trace elements in the CNS for the synaptic transmission and signaling cascades (Bitanihirwe and Cunningham, 2009; D'Ambrosi and Rossi, 2015).

2 | MATERIALS AND METHODS

2.1 | BBV displaying human MC_4R

Recombinant baculoviruses of human MC_4R were constructed and generated as described previously by Veiksina *et al*. (2010) using homologous recombination via transfection of *Spodoptera frugiperda* (Sf9) cells (Invitrogen Life Technologies, UK, Cat# 11496–015; maximum of 30 passage was used). The International Cell Line Authentication Committee does not list any of the cell lines used in this study as commonly misidentified cell lines. None of them was authenticated after purchase. The baculoviruses were amplified (until achieving 10^8 ivp/ml), and the titer was determined by a cell size-based assay (Laasfeld, Kopanchuk, and Rinken, 2017). This high-titer virus was used to infect Sf9 cells at a density of 2×10^6 cells/ml with a multiplicity of infection (MOI) of 5 for the production of BBV preparation. The infected cells were cultured at 27°C in serum-free EX-CELL 420 medium (Sigma-Aldrich, Cat# 14420C) without antibiotics in a non-humidified incubator for 72 h. For the collection of BBV, the cells were separated by centrifugation at 1,600 g for 10 min, and the supernatant was centrifuged at 48,000 g for 40 min at 4°C. The pellet was suspended in buffer A (pH 7.4), which contained 11 mM Na-HEPES (Amresco, Cat# 0511-250G), 135 mM NaCl (AppliChem, Cat# A2942, 1,000), 5 mM KCl (AppliChem, Cat# A358, 1,000), 0.1% Pluronic F-127 (Sigma-Aldrich, Cat# P2443-250G), and Complete EDTA-Free

Protease Inhibitor Cocktail (according to the manufacturer's description, Roche Applied Science, Cat# 1,187,358,001), at a ratio of 1:50 as the initial cell suspension volume. Prior to that, the pellet was washed twice – first with buffer A plus 1 mM EDTA (Merck, Cat# 6381–92–6) and second only with buffer A. Aliquots of the BBV preparation was stored at −90°C.

2.2 | FA-BBV assay system

The Cy3B-labeled UTBC101 (Cy3B-Nle-c[Asp-His-DNal(2')-Arg-Trp-Lys]-NH_2), UTBC102 (Ac-Lys(Cy3B)-c[Asp-His-DNal(2')-Arg-Trp-Lys]-NH_2) (CEPEP EESTI, Estonia), and TAMRA-labeled NDP-α-MSH (TAMRA-Ser-Tyr-Ser-Nle-Glu-His-DPhe-Arg-Trp-Gly-Lys-Pro-Val-NH_2) (AnaSpec, Cat# AS-60564–1) were characterized as described previously (Veiksina *et al*., 2010; Link *et al*., 2017). Aliquots of those ligands were stored at −90°C in DMSO. The FA-based assay with the implementation of the homogenous BBV was set up as described previously (Veiksina *et al*., 2015). In brief: experiments were carried out in buffer A with modifications described in the specific assay setups in a final volume of 100 µl using 96-well half area, flat-bottom polystyrene NBS microtiter plates (Corning, Cat# 3,993). Reactions were started by the addition of the BBV preparation to the fluorescent ligand with or without competing ligands and modulators. The measurements were performed in kinetic mode at 27°C on a Synergy™ NEO (BioTek) microplate reader using an optical module with an excitation filter at 530 nm (slit 25 nm) and dual emission filters at 590 nm (slit 35 nm). Parallel polarized light was used for the excitation followed by the dual detection of emission in the parallel ($I_{||}$) and perpendicular ($I_{\perp}$) plane. The instrument sensitivity ratio (G factor) toward the dual detection was corrected with erythrosine B (Thompson *et al*., 2000). The fluorescence anisotropy values were calculated as parameter FA using the following equation: $FA = (I_{||} - I_{\perp})/(I_{||} + 2I_{\perp})$, where the fluorescence intensities ($I_{||}$, $I_{\perp}$) were background corrected a priori. The specific binding (ΔFA) was defined as the difference between FA values of the total and non-specific binding of the fluorescent ligands. The total binding was measured in the absence and non-specific binding in the presence of a potent MC_4R antagonist, 3 µM SHU9119 (Tocris Bioscience, Cat# 3420/1).

2.2.1 | Saturation binding and dissociation assays

The binding of the fluorescent ligand to MC_4R was determined by varying the concentrations of MC_4R (0–14.6 nM for UTBC101; 0–52 nM for UTBC102) in buffer A plus 1 mM $MgCl_2$ (≥99.5%, AppliChem, Cat# 44250500), 2 mM $CaCl_2$ (≥99.5%, AppliChem, Cat# A18730500), and 1 mM EDTA (Merck, Cat# 6381–92–6). The binding reactions were started by the addition of the BBV preparation of MC_4R to two different concentrations of the fluorescent ligand (0.4, 4 nM UTBC101; 0.5, 7 nM UTBC102) in the presence (non-specific binding) or absence (total binding) of 3 µM SHU9119. The binding of UTBC101 and UTBC102 was measured for 3 h and 0.5 h, respectively. Next, the dissociation was initiated with 3 µM SHU9119 and measured for 6 h and 0.5 h, in the case of UTBC101 and UTBC102, respectively. The reaction parameters (affinity, kinetic parameters) and the concentration of ligand-specific MC_4R-binding sites ($[R]_{stock}$) in the BBV preparation were estimated by global fitting of the data (Veiksina, Kopanchuk, and Rinken, 2014). This simultaneous fitting of total and non-specific binding data takes into account the ligand depletion by both binding processes.

2.2.2 | Divalent metal ion modulated binding assay

The modulation of fluorescent ligand binding by divalent metal ions was determined at a fixed concentration of the fluorescent ligand (0.3 nM UTBC101, 6.2 nM UTBC102, 6.2 nM TAMRA-NDP-α-MSH) and the MC_4R (0.6 nM, 11.2 nM, and 11.2 nM, respectively) in the presence or absence of EDTA (in the range from 0.01 to 1 mM, Merck, Cat# 6381-92-6). Non-specific binding was determined in the presence and total binding in the absence of 3 µM SHU9119. Buffer A plus 1 mM $CaCl_2$ was used as the assay buffer if not stated otherwise. Divalent metal ions used for the experiment were diluted from stock solutions of $MgCl_2$ (≥99.5%, AppliChem, Cat# 4425,0500), $CaCl_2$ (≥99.5%, AppliChem, Cat# A1873,0500), $Sr(NO_3)_2$ (98%, Acros Organics, Cat# 438520010), $BaCl_2$ (ReaChim, Cat# 020110), $MnCl_2$ (>99%, AppliChem, Cat# A2087,0100), $ZnSO_4$ (99%, ReaChim, Cat# 220,128) or $CuCl_2$ (99.99%, Sigma-Aldrich, Cat# 467847-50G). The salt solutions were added to the reaction medium at the start of the ligand-binding reaction or after the equilibrium had been achieved (after 3 h for UTBC101, 0.5 h for UTBC102, and 1.5 for TAMRA-NDP-α-MSH). The details of the particular experiments are shown in the Figures.

2.3 | Baculoviruses expressing the bacmam-$EpacH^{187}$ biosensor

The expression vector pcDNA3.1(+)-mTurq2Δ_Epac(CD,ΔDEP, Q270E)_td^{cp173}Ven (referred to as $Epac^{H187}$ throughout the text) (Klarenbeek, Goedhart, van Batenburg, Groenewald, and Jalink, 2015) containing the desired gene of the FRET-based cAMP biosensor was kindly provided by Dr Kees Jalink. The $Epac^{H187}$ construct was modified for use in the BacMam system as previously described (Mazina, Allikalt, *et al*., 2015a; Mazina, Luik, Kopanchuk, Salumets, and Rinken, 2015b). In brief, the $Epac^{H187}$ construct under control of the cytomegalovirus promoter was cloned into the pFastBac™1 vector (Invitrogen life technologies, Cat# 10359–016), replacing its polyhedrin promoter. The restriction enzymes (Thermo scientific) FastDigest RruI (Cat# FD2154) and FastDigest EcoRI (Cat# FD0274) were used for pcDNA3.1(+) and EcoRI (Cat# ER0271) and Eco105I (SnaBI, Cat# ER0401) for pFastBac™1. The resulting

pFastBac- Epac^{H187} construct was incorporated into the recombinant Sf9 cell genome (bacmid) for the production of BacMam virus via transfection. Sf9 cells were also used for virus amplification and titer determination (Laasfeld *et al*., 2017). Aliquots of the amplified BacMam virus were stored at −90°C.

2.4 | CHO-K1 cell line stably expressing human MC_4R

Chinese hamster ovary (CHO-K1) cells (ATCC, LGC Standards, Germany, RRID: CVCL_0214; maximum of 26 passage was used) were used to develop a modified cell line stably expressing MC_4R. The pcDNA3.1 + expression vectors (Invitrogen) containing the desired gene of the human wild-type MC_4R (Missouri S&T cDNA Resource Center, Cat# #MCR0400000) were transfected into the cells using ExGen 500 (Fermentas) according to the manufacturer's instructions. Post-transfection, the cells were subjected to 500 µg/ml geneticin (G418) selection (PAA Laboratories, Cat# P25-011). Selected G418 resistant clonal stable cultures were tested for receptor expression with known melanocortin ligands by receptor activation (using cAMP biosensor BacMam-Epac^{H187}). Henceforth the CHO-K1-MC_4R cells (maximum of 37 passage was used) were maintained in the presence of 400 µg/ml of G418. The cells were cultivated in high glucose Dulbecco's Modified Eagle's Medium (DMEM) (Sigma-Aldrich, Cat# D5796-500Ml) supplemented with 10% fetal bovine serum (Sigma-Aldrich, Cat# F7524-500Ml), 100 U/ml penicillin, and 0.1 mg/ml streptomycin (PAA Laboratories, Cat# A5955-100Ml) at 37°C in a humidified incubator with 5% CO_2.

2.5 | cAMP activation assay

The BacMam-Epac^{H187} biosensor assay to measure the activation of MC_4R in CHO-K1-MC_4R cells was performed as described previously with some modifications (Mazina, Allikalt, *et al*., 2015a; Mazina, Luik, *et al*., 2015b). In brief, mammalian cells were treated with the BacMam viral stock (MOI:9–25) in growth medium containing 12 mM sodium butyrate (Sigma-Aldrich, Cat# 303410-100G) and seeded on a black clear-bottom 96-well cell culture plate (Corning Life Sciences, Cat# 3340) at the density of 1×10^5 cells/well in a 100 µl volume. The transduced cells were cultured for 30 h at 30°C in a humidified CO_2 incubator for recombinant protein production. Prior to the experiment (0.5 h), the cells were washed, and buffer A plus 1 mM $CaCl_2$ without protease inhibitors was used to replace the medium. The fluorescence intensities of the cAMP sensors were registered before and after cell stimulation with a ligand and/or a modulator using a Synergy™ NEO (BioTek) microplate reader. The biosensors were excited at 420/50 nm, and emissions of the donor and the acceptor fluorophores were measured simultaneously at 485/20 and 540/25 nm, respectively. The change in cAMP concentration is proportional to the change in the emission intensity ratio of the donor and the acceptor fluorophores, which is calculated as follows: $\Delta FRET = [(I_0^{acceptor}/ I_0^{donor})-(I_t^{acceptor}/I_t^{donor})]/(I_0^{acceptor}/I_0^{donor})$. The $I_0^{acceptor}$, I_0^{donor}, and $I_t^{acceptor}$, I_t^{donor} refer to the fluorescence emission intensities of the acceptor and donor fluorophores before and after cell stimulation, respectively.

2.6 | Analysis of metal content using ICP-MS

The analyzed preparations were diluted 100-fold with 2% HNO_3 (Carl Roth, ROTIPURAN® Supra, Cat# HN50.2). The content of metals was measured by inductively coupled plasma mass spectrometry (ICP-MS) Agilent 8800 and modeled using MassHunter software (RRID: SCR_015040). ^{39}K and ^{40}Ca were measured using 8 ml/min of H_2, and ^{51}V, ^{52}Cr, ^{56}Fe, ^{63}Cu, were measured using 6 ml/min of He in the collision/reaction cell in MS/MS mode. ^{23}Na, ^{24}Mg, ^{55}Mn, ^{59}Co, ^{61}Ni, ^{66}Zn, ^{85}Rb, ^{88}Sr, ^{111}Cd ^{137}Ba, and ^{208}Pb were measured using NoGas mode. Indium (measured as ^{115}In in all measurement modes) in 2% HNO_3 was used as an internal standard that was added using a T-piece "online", and NIST SRM 1643f (Trace Elements in Natural Water) was used as a quality control standard.

2.7 | Materials availability

The samples of baculoviruses with MC_4R, UTBC101, and UTBC102 are available upon reasonable request sent to Sergei Kopanchuk (sergei.kopanchuk@ut.ee) and Ago Rinken (ago.rinken@ut.ee).

2.8 | Data analysis

The data management of ligand binding and functional assays was performed with the software Aparecium 2.0.20 developed in our laboratory and available at http://www.gpcr.ut.ee/software.html. The data analyses were performed in GraphPad Prism 5.04 (GraphPad Software, USA, RRID: SCR_002798) with built-in or user-defined (Veiksina *et al*., 2014) algorithms. The user-defined algorithms were used to analyze the saturation and association kinetic-binding assays (Veiksina *et al*., 2014). The one-phase exponential function was used to analyze the dissociation kinetics if not stated otherwise. Three parameters logistic function or Schild analysis was used to analyze the cAMP activation assays if not stated otherwise. The data are presented as the mean ± standard deviation of at least three independent experiments ($n \geq 3$) if not stated otherwise. The "n" indicates the number of experiments performed on different days using new aliquots of BBV stock solution for ligand binding and ICP-MS experiments or the number of assay preparations of cells from different passages for functional experiments. No ethical approval was needed for this study. No animals nor patients were involved and therefore the study was not

pre-registered, no randomization and other study design attributes were performed. In this study, statistical methods to predetermine the sample size were not employed, blinding was not performed and test for outliers was not conducted. Assessment of the normality of data was carried out using D'Agostino-Pearson normality test. Non-parametric Mann–Whitney U test that does not assume normal distribution of the data was used to assess the statistically significant differences in the medians of two groups ($p < .05$).

3 | RESULTS

3.1 | Modulation of the fluorescent ligand-binding level of MC_4R

3.1.1 | The effect of EDTA on the ligand-binding level

We have previously successfully applied the FA-based assay for the characterization of ligand binding to MC_4R using different fluorescent ligands (Veiksina *et al*., 2010, 2014; Link *et al*., 2017). In this study, we discovered that even low concentrations of EDTA in the presence of 1 mM Ca^{2+} substantially improved the level of the FA signal, which corresponds to fluorescent ligand binding to MC_4R in BBV particles. This FA signal increase was studied using two fluorescent ligands, one of which has a higher affinity (UTBC101) and the other faster kinetics (UTBC102) (Link *et al*., 2017). Determination of the binding properties of these fluorescent ligands in the presence of EDTA revealed apparent K_d values of 0.23 ± 0.07 nM and 3.3 ± 0.9 nM for UTBC101 and UTBC102, respectively (Figure 1). These values are in good agreement with the results obtained in the experiments without EDTA (Link *et al*., 2017). Thus, under conditions where the amount of added EDTA was substantially lower than the amount of Ca^{2+}, the EDTA had no influence on the ligand-binding affinity.

The increase in specific ligand binding caused by EDTA could be detected in the presence of 1 mM free Ca^{2+} for UTBC101 as well as for UTBC102 (Figure 2a). Without the addition of Ca^{2+}, no specific ligand binding was detected, and the addition of EDTA had no substantial effect (Figure 2a). In the presence of Ca^{2+}, the addition of only 10 μM EDTA caused clear increase in FA (Figure 2a, blue boxes). This low concentration does not considerably affect the free concentration of Ca^{2+} in the buffer, which was set on 1 mM. The increase in the ΔFA level caused by EDTA was more than twice (230 ± 24%) for the high-affinity ligand UTBC101, whereas, for UTBC102, which has lower affinity for MC_4R, the increase remained on the level of 126 ± 15%. The increase in the EDTA concentration to the level of 1 mM with a concurrent increase in the total Ca^{2+} concentration to the level of 2 mM (to retain the 1 mM free Ca^{2+} concentration) did not cause significant additional changes in the ΔFA level (Figure 2a, yellow boxes). This indicates that 10 μM EDTA was sufficient to diminish the inhibitory effect present in our assay system. Therefore, this EDTA concentration was used in the following experiments, if not stated otherwise.

3.2 | The stimulatory effect of different divalent metal ions on the ligand-binding level

It is known that Ca^{2+} ions are essential for high-affinity ligand binding to MC_4R (Kopanchuk *et al*., 2005). To understand whether the EDTA complex formation with Ca^{2+} may influence also the fluorescent ligand binding, we determined the effect of different concentrations of Ca^{2+} in the presence of 10 μM EDTA. The binding of 0.3 nM UTBC101 reached its maximal level at 1 mM Ca^{2+} and remained there with the additional increase in the Ca^{2+} concentration up to 10 mM (Fig. S1). Therefore, in the following experiments, the added free Ca^{2+} concentration was kept at 0.9–1.0 mM, if not stated otherwise. In addition to Ca^{2+}, we also studied other divalent metal ions with similar biochemical properties, Mg^{2+}, Ba^{2+}, Sr^{2+}, and Mn^{2+}, to evaluate whether the effect of Ca^{2+} on ligand binding to MC_4R was unique. None of studied ions induced the same level of UTB101 binding as Ca^{2+}. The best results were obtained with Sr^{2+}, which was followed by Mn^{2+}, Ba^{2+}, Mg^{2+} (Figure 2b). The addition of 10 μM EDTA significantly increased the FA-specific-binding signal of UTBC101 in the presence of most of these metal ions (Figure 2b), but the efficacy order for the ions remained unchanged also after the addition of EDTA. Further increases in the EDTA concentration up to 1 mM (salt concentrations were increased to 2 mM to retain the 1 mM of the free ion concentrations) did not cause principal changes in the FA-specific-binding signal (Figure 2b).

3.3 | Identification of metals in the ligand-binding assay system

The EDTA-dependent increase in ligand binding to MC_4R indicated that the inhibitory effect could be caused by some metal ions, which form tight complexes with EDTA and can be originated from the samples of our assay system. ICP-MS revealed that the BBV preparation of MC_4R contained, in addition to Na and K (buffer components in millimolar concentration), substantial amount of Mg, Ca, Zn, Cu, and Mn (Figure 2c). Other metals studied (Rb, Sr, Ba, V, Cr, Fe, Co, Ni, Cd, Pb) were absent or could not be reliably quantified because their concentrations remained below 0.1 μM. Ca^{2+} ions could be ruled out from the list of inhibitors because of their essential role in the high-affinity ligand binding to MC_4R. Thus, Mg^{2+}, Mn^{2+}, Zn^{2+}, and Cu^{2+} ions became the main suspects.

3.4 | The inhibitory effect of the metal ions on the ligand-binding level

The influence of Mg^{2+}, Mn^{2+}, Zn^{2+}, and Cu^{2+} ions on fluorescent ligand binding to MC_4R was studied in the absence and presence of 1 mM Ca^{2+}. Without Ca^{2+}, none of the studied ions at up to 200 μM concentrations had a clear stimulatory effect on the binding of UTBC101 (Figure 2d, blue boxes), which remained almost on the level of non-specific binding. The addition of submillimolar concentration

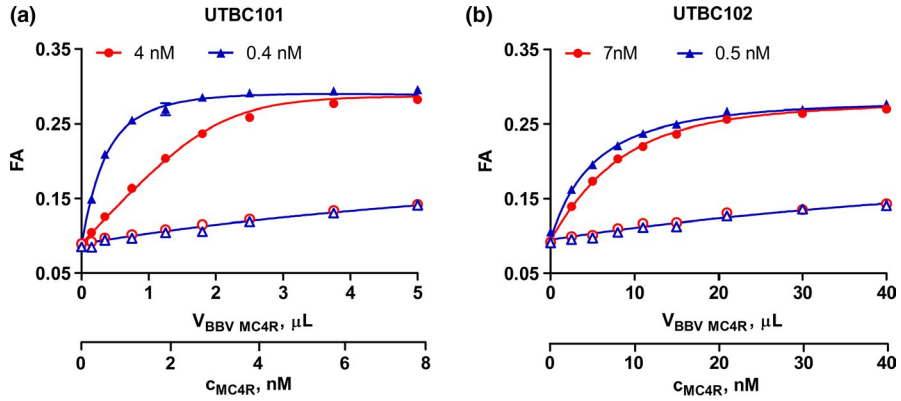

	K_d (nM)	k_{off} (min^{-1})	k_{on} (x 10^7 $M^{-1}min^{-1}$)
UTBC101	0.23 ± 0.07	(4.6 ± 0.6) x 10^{-3}	2.1 ± 0.5
UTBC102	3.3 ± 0.9	(1.1 ± 0.3) x 10^{-1}	3.6 ± 0.7

FIGURE 1 Binding curves of fluorescent ligands to MC_4R. UTBC101 at concentrations of 0.4 and 4 nM (a) and UTBC102 at concentrations of 0.5 and 7 nM (b) were incubated with increasing amounts of the MC_4R preparation in budded baculoviruses (BBV). The binding was measured in the absence (filled symbols, total binding) and presence of 3 µM SHU9119 (open symbols, non-specific binding) after incubation for 3 h (a) or 0.5 h (b). The binding of the ligands was characterized as the change in fluorescence anisotropy (FA) values. The graphs show a representative experiment of at least three independent experiments performed in duplicate. The mean ± *SD* of the ligand-binding parameters (K_d, k_{on}, and k_{off}) estimated by global data fitting of the kinetic data as described in Materials and Methods, are shown in the table (n = 3)

of EDTA, which had a stimulatory effect in the presence of Ca^{2+}, had no such effect in this system (Figure 2e, blue boxes). In the presence of 1 mM Ca^{2+}, UTBC101 binding to MC_4R was not significantly influenced by the addition of Mg^{2+} and Mn^{2+} at concentrations up to 200 µM, whereas the addition of Zn^{2+} and Cu^{2+} ions caused significant inhibition already at the 10 µM concentration (Figure 2d, orange boxes). Zn^{2+} reduced ΔFA values to the level of 32 ± 10% and Cu^{2+} to the level of non-specific binding. The addition of 100 µM EDTA in the presence of 1 mM Ca^{2+} doubled the level of the ΔFA values of specific ligand binding (214 ± 21%), which remained as such also in the presence of 200 µM Mg^{2+} or Mn^{2+} ions (Figure 2e, orange boxes). However, the effect of EDTA was not visible in case of Zn^{2+} and Cu^{2+} ions as the UTBC101 binding remained at the same low level (Figure 2e, orange boxes). These results confirmed that Zn^{2+} and Cu^{2+} could be the ions that inhibit ligand binding to MC_4R, and their removal with EDTA can at least partially restore the level of ligand binding.

3.5 | Modulation of fluorescent ligand-binding kinetics to MC_4R

3.5.1 | The effect of Zn^{2+} and Cu^{2+} on ligand-binding kinetics

To gain insights into the inhibitory mechanism of Zn^{2+} and Cu^{2+} ions, we studied the modulation of the kinetic aspects of ligand binding to MC_4R by these ions. In the association kinetic experiments, 10 µM EDTA caused a clear enhancement of the specific binding of 0.3 nM UTBC101 in comparison to the control, where only the buffer with 1 mM Ca^{2+} was used (Figure 3, a and b). In contrast, Zn^{2+} and Cu^{2+} ions inhibited the binding of UTBC101 in a concentration-dependent manner. Substantial inhibition of the ΔFA values was evident already at 10 µM Zn^{2+} and 0.3 µM Cu^{2+} (Figure 3, a and b). In addition to inhibition of total fluorescent ligand binding, Zn^{2+}, and Cu^{2+} ions also changed the basal FA levels corresponding to the non-specific ligand binding determined in the presence of 3 µM SHU9119. These changes were taken into account in the calculation ΔFA values of the specific binding presented in Figure 3.

The time-dependent decrease in the ΔFA values could also be observed if Zn^{2+} and Cu^{2+} ions were added after the pre-incubation of UTBC101 with MC_4R when the receptor-ligand complexes had been formed (Figure 3, c and d). The rate and level of dissociation of UTBC101 from complexes with the receptors depended on the concentration of the added ions. The increase in Zn^{2+} concentration from 1 to 32 µM increased the dissociation rate of UTBC101 by 20-fold, changing the apparent dissociation rate constant k_{off} from 0.006 ± 0.002 min^{-1} ($\tau_{1/2}$ = 116 min) to 0.12 ± 0.06 min^{-1} ($\tau_{1/2}$ = 6 min), respectively. A similar Zn^{2+} and Cu^{2+} concentration-dependent dissociation was caused in the case of UTBC102, which showed lower affinity binding to MC_4R (Figure 3, e and f). The need to use high receptor concentrations for this ligand and the ligand's fast kinetics did not allow the performance of classical concentration-dependent inhibition experiments to estimate the dissociation rate constants. However, the consecutive addition of the ions indicated a clear concentration dependence of the effect for UTBC102 (Figure 3, e and f). In addition to UTBC102, we could measure the influence of Zn^{2+} and Cu^{2+} ions on the dissociation rate of another lower-affinity fluorescent ligand TAMRA-NDP-α-MSH. However,

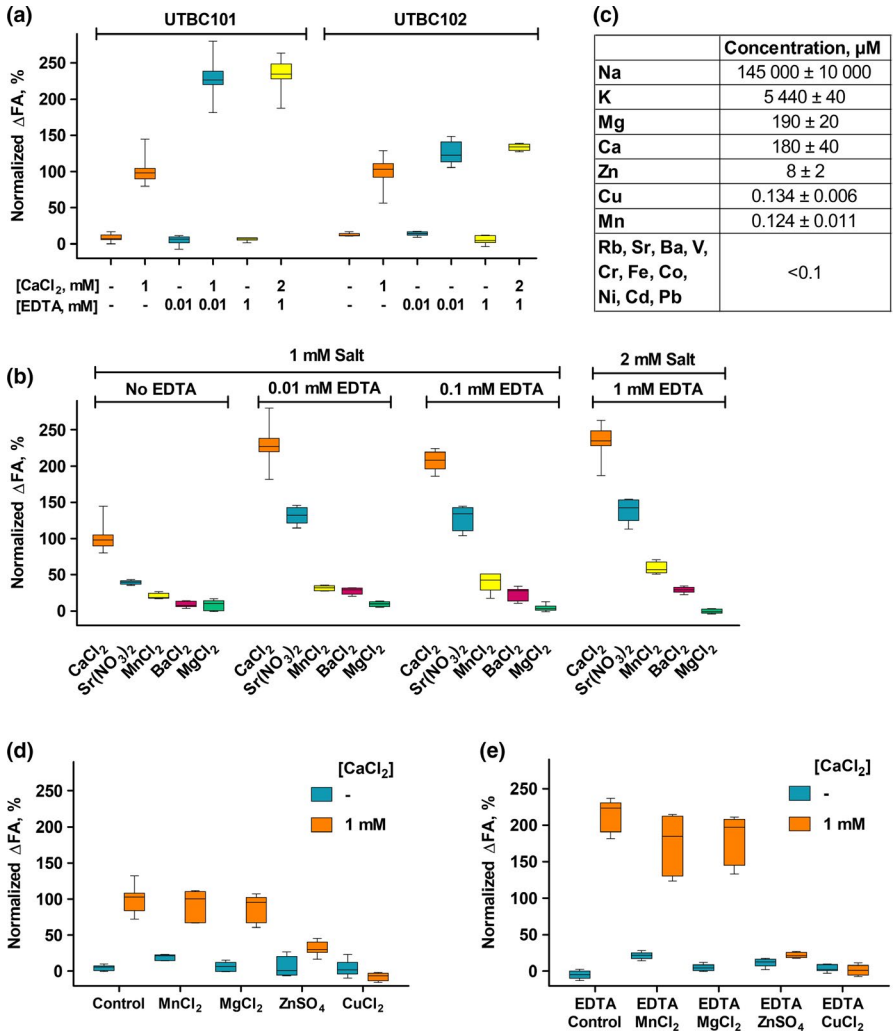

FIGURE 2 Effects of EDTA and different salts on the binding of fluorescent ligands to MC_4R. (a) The effect of different concentrations of EDTA on the specific binding of UTBC101 and UTBC102 to MC_4R in the absence and presence of Ca^{2+}. (b) Effects of different salts on the specific binding of UTBC101 to MC_4R in the presence of different concentrations of EDTA. (c) The concentration of metals (as ions) in the stock preparation of MC_4R in budded baculoviruses (BBV) determined with ICP-MS (mean ± *SD*, *n* = 3). (d) Effects of different divalent metal salts on the binding of UTBC101 to MC_4R in the absence or presence of Ca^{2+}. The concentration of salts used: 0.2 mM $MnCl_2$, 0.2 mM $MgCl_2$, 0.01 mM $ZnSO_4$, 0.01 mM $CuCl_2$, 1 mM $CaCl_2$. (e) Effects of different salts on the binding of UTBC101 to MC_4R in the presence of EDTA and the absence or presence of Ca^{2+}. The concentration of salts used: 0.2 mM $MnCl_2$, 0.2 mM $MgCl_2$, 0.02 mM $ZnSO_4$, 0.02 mM $CuCl_2$, 1 mM $CaCl_2$. The concentration of EDTA was 0.1 mM for the Control, $MgCl_2$, $MnCl_2$, and 0.01 mM for $ZnSO_4$, $CuCl_2$. In all of the experiments, 0.3 nM UTBC101 or 6.2 nM UTBC102 was used with 0.6 or 11.2 nM MC_4R, respectively. The specific binding of fluorescent ligands was characterized by the change in ΔFA levels normalized to the binding signal obtained in the presence of 1 mM $CaCl_2$ without EDTA. The box-plots show data of at least three independent experiments ($n \geq 3$) performed in duplicates. The box-plots show median, upper quartile 75th percentile, and lower quartile 25th percentile, and whiskers show maximum and minimum data values

the low affinity of the ligand requires the use of very big amounts of receptors and therefore only a proof of principle experiment ($n = 1$) could be performed (Fig. S2). Binding of this ligand was also inhibited by Zn^{2+} and Cu^{2+}, and restored by the addition of EDTA (Fig. S2, a and b). The apparent potencies of the ions to inhibit the binding of UTBC101 and UTBC102 to MC_4R depended on the ligand used (Fig. S3). The UTBC101 binding was inhibited by Zn^{2+} with $pIC_{50} = 5.38 \pm 0.05$, and by Cu^{2+} with $pIC_{50} = 7.02 \pm 0.09$. In the case of UTBC102, about 20 times higher receptor concentration had to be used, and the apparent pIC_{50} value for Zn^{2+} was 6.32 ± 0.06 and for Cu^{2+} was 5.82 ± 0.13 (Fig. S3).

3.5.2 | Reversibility of the inhibitory effect of Zn^{2+} and Cu^{2+}

The inhibitory effects of Zn^{2+} and Cu^{2+} ions on fluorescent ligand binding was partially reversible by the addition of excess EDTA (100 µM) (Figure 3c–f). In the case of up to 3 µM concentrations of Zn^{2+}, the addition of 100 µM EDTA fully restored the binding of UTBC101. If the receptors were treated with higher concentrations of Zn^{2+}, the addition EDTA could not fully restore the original ΔFA levels, indicating a partial loss of UTBC101 binding (Figure 3c). In the case of Cu^{2+}, the binding of UTBC101 could not

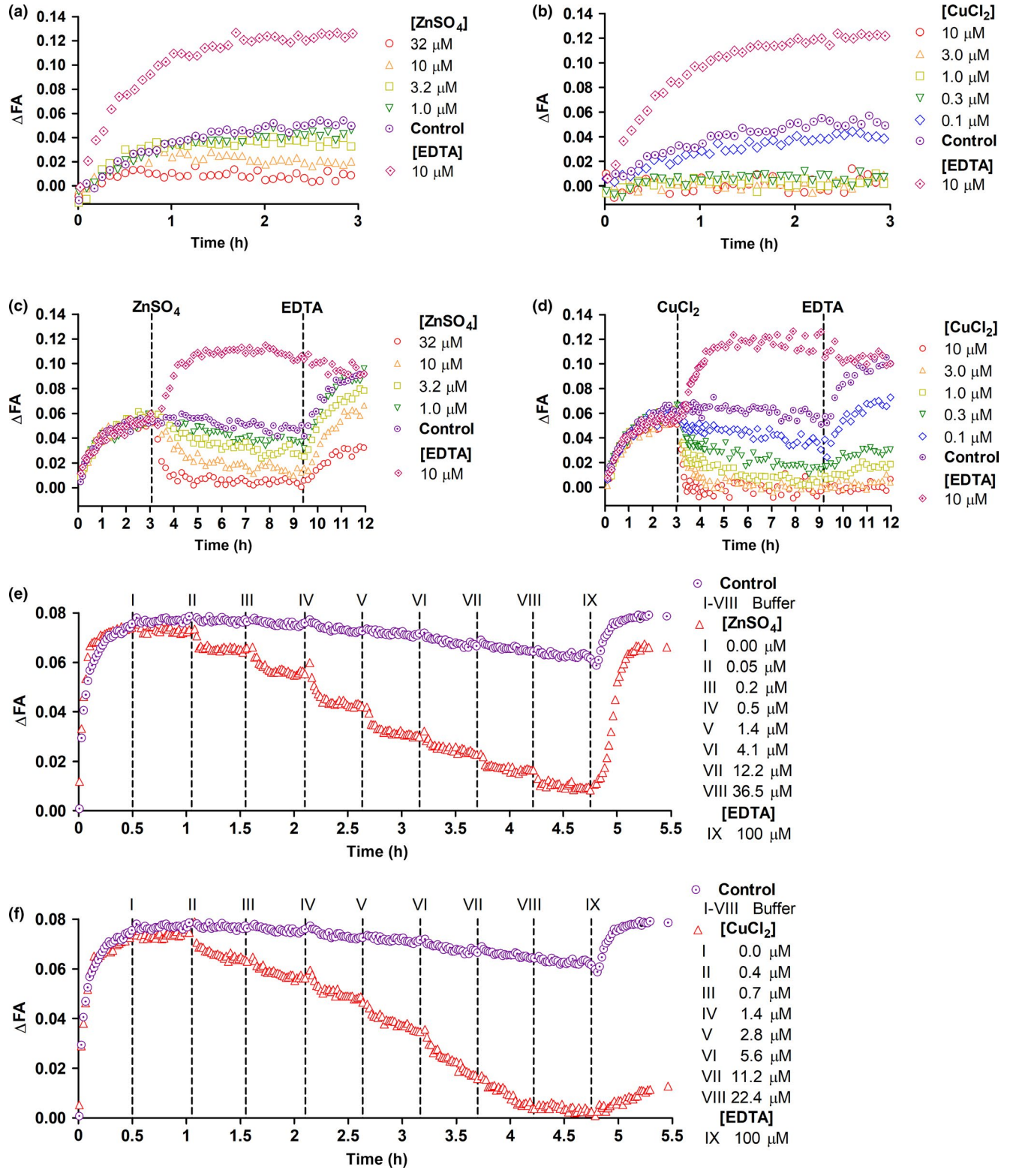

FIGURE 3 Effects of Zn^{2+} and Cu^{2+} on the binding kinetics of UTBC101 (a–d) and UTBC102 (e and f) to MC_4R. Different concentrations of $ZnSO_4$ (a) and $CuCl_2$ (b) or 10 μM EDTA (a and b dotted diamonds) together with 1 mM $CaCl_2$ were added before starting the binding reaction of 0.3 nM UTBC101 toward 0.6 nM MC_4R. UTBC101 was incubated with MC_4 receptors in the presence of 1 mM $CaCl_2$ for 3 h, after which the indicated concentrations of $ZnSO_4$ (c) or $CuCl_2$ (d) or 10 μM EDTA (c, d dotted diamonds) were added. The 6.2 nM UTBC102 was incubated with MC_4R in the presence of 1 mM $CaCl_2$ for 0.5 h, after which at every 0.5-h time point (I-VIII), $ZnSO_4$ (e triangles), and $CuCl_2$ (f triangles) were added to achieve the indicated salt concentration. As a control, the same amount of buffer was added at these time points (e, f dotted rings). The reversibility of the salt effects were measured by the addition of 100 μM EDTA about 6 h (c and d) or 4 h (e–f IX) after the start of the experiment. The binding of ligands was characterized as the change in ΔFA values in time. The graphs show the data points from representative experiments of three independent experiments (n = 3)

be fully restored with EDTA even at the lowest 0.1 μM ion concentration, and 3 μM Cu^{2+} caused practically irreversible inhibition of the binding (Figure 3d). A similar pattern of partial reversibility with EDTA was also found in the case of UTBC102 (Figure 3, e and f) and TAMRA-NDP-α-MSH (Fig. S2), whereas the reversible fraction was larger for these ligands.

3.6 | Modulation of MC_4R-mediated signal transduction

3.6.1 | The effects of ligands on the signal transduction of MC_4R

To study MC_4R-mediated signal transduction, we generated a stable CHO-K1 cell line expressing human MC_4R. The activation of MC_4R, which is coupled to the Gs-pathway, leads to increased cAMP production, which can be measured in living cells using the FRET-based $Epac^{H187}$ biosensor (Klarenbeek *et al*., 2015). We used the BacMam system for expression of the biosensor, and changes in the level of cAMP were detected from the changes in the ΔFRET values. The full agonist of the MC_4R, NDP-α-MSH (Haskell-Luevano *et al*., 1997), caused a concentration-dependent increase in the ΔFRET values of the biosensor (Figure 4), and the maximal level was achieved within 30 min. In contrast, in naive CHO-K1 cells, which were used as a control, 1 nM NDP-α-MSH did not cause this kind increase in the ΔFRET values (Figure 5b, squares and diamonds). Full activation of the MC_4R system was achieved also with the fluorescently labeled derivate TAMRA-NDP-α-MSH (Figure 4). Among the new fluorescent ligands, UTBC102 behaved as a classical partial agonist, achieving a 68 ± 5% level of activation in comparison to NDP-α-MSH. The second novel ligand, UTBC101, had only minimal agonistic activity, achieving only a 22 ± 2% level of activation in comparison to the full agonist. It is interesting to note that HS024, which is known as the silent antagonist for MC_4R (Kask *et al*., 1998), also showed minimal agonistic activity in our system, generating an activation level of 19 ± 3% in comparison to the full agonist (Figure 4). The potencies of the ligands are listed in the table of Figure 4.

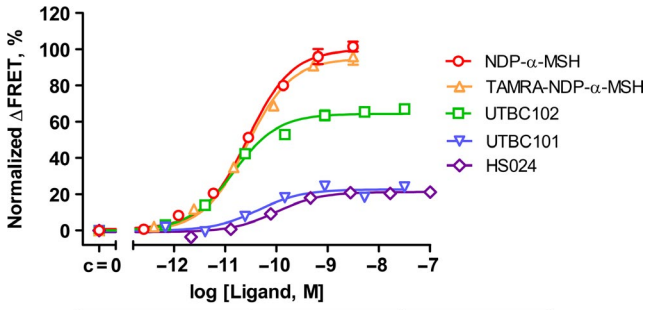

Ligand	log [EC_{50}] ± SD		Efficacy ± SD, %	
NDP-α-MSH	−10.7	0.2	100	-
TAMRA-NDP-α-MSH	−10.9	0.3	96	2
UTBC102	−10.8	0.2	68	5
UTBC101	−10.7	0.3	22	2
HS024	−10.3	0.5	19	3

FIGURE 4 Influence of different MC_4R ligands on the activation of cAMP production in CHO-K1-MC_4R cells. The ΔFRET values were measured 30 min after the addition of the indicated concentrations of ligands to CHO-K1-MC_4R cells expressing the cAMP biosensor BacMam-$Epac^{H187}$. The data points shown are from a representative experiment of at least three independent experiments ($n \geq 3$) performed in triplicate and normalized to the maximal NDP-α-MSH signal. The mean ± *SD* of parameters for ligand-specific effects are shown in the table

3.6.2 | The effect of Zn^{2+} and Cu^{2+} ions on MC_4R-mediated signal transduction

The addition of Zn^{2+} ions without ligands to CHO-K1 cells expressing MC_4R caused a clear concentration-dependent change in the ΔFRET values, indicating the accumulation of cAMP (Figure 5a, triangles), whereasthe response in naive CHO-K1 cells was marginal (Figure 5b, triangles). In both cell lines, the ΔFRET values were normalized to the forskolin-induced cAMP response. The effect of Zn^{2+} ions in the cells with MC_4R was agonistic, achieving a 93 ± 6% level of activation in comparison to the full agonist NDP-α-MSH (Figure 5a, triangles). Half of the maximal response was achieved at a 1.1 μM Zn^{2+} concentration (pEC_{50} 5.95 ± 0.12). The addition of Cu^{2+} ions to the cells expressing MC_4R caused more complex responses: at lower concentrations (up to 1.5 μM) of Cu^{2+}, the ΔFRET values increased to the level of 33 ± 9%, whereas at higher concentrations of Cu^{2+}, the ΔFRET signal decreased even below baseline (Figure 5a, circles). In the naive cells without MC_4R, Cu^{2+} ions caused only a moderate increase in ΔFRET values, which remained in the same range as in the case of Zn^{2+}, and there was no drop of the signal at higher Cu^{2+} concentrations (Figure 5b, circles). In cells expressing MC_4R, 1 nM NDP-α-MSH induced the maximal agonistic response, which was only moderately influenced by Zn^{2+} and Cu^{2+} ions (Figure 5a, squares and diamonds). In the cells without MC_4R, 1 nM NDP-α-MSH did not affect the presence or absence of Zn^{2+} or Cu^{2+} (Figure 5b, squares and diamonds).

3.6.3 | The effect of Zn^{2+} and Cu^{2+} ions on ligand-induced responses

As Zn^{2+} ions alone induced almost the same level of activation response of MC_4R as full agonists, we studied the influence of the ion on the NDP-α-MSH-stimulated accumulation of cAMP (Figure 5c). A slight increase over the level of the maximal response of the full agonist NDP-α-MSH was observed in the presence of 3 μM or higher concentrations of Zn^{2+}, but this did not exceed 132% at any concentrations studied (Figure 5c). Concurrently, Zn^{2+} at all studied concentrations did not cause changes in the potency of the NDP-α-MSH in activating the cAMP pathway. As Cu^{2+} ions alone induced a biphasic effect on the accumulation of cAMP, the effects toward the agonist inducing signaling were also complex. The addition of low concentrations of the ion (up to 4 μM) caused an upward shift in

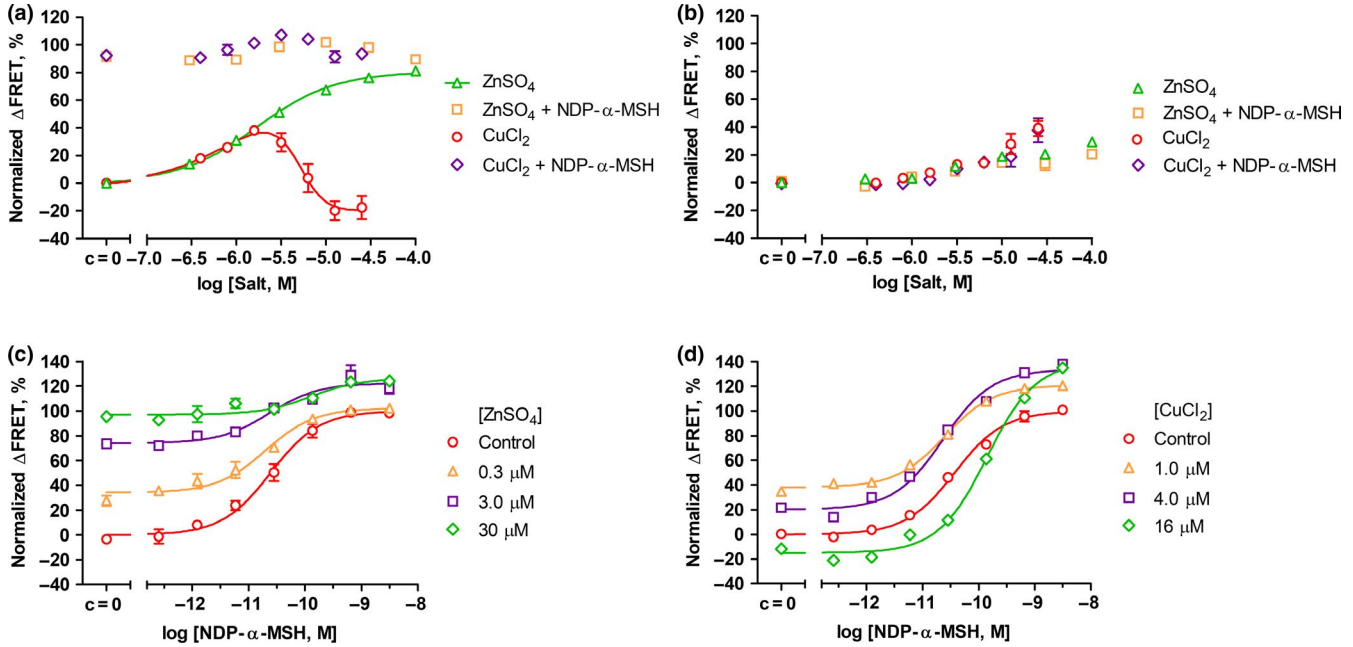

FIGURE 5 Effects of Zn^{2+} and Cu^{2+} on the activation of cAMP production in CHO-K1 cells with and without MC_4R. The ΔFRET values of CHO-K1-MC_4R (a, c, and d) and CHO-K1 (b) cells expressing the cAMP biosensors BacMam-Epac^{H187} were measured 30 min after the addition of different concentrations of $ZnSO_4$ and $CuCl_2$ with and without NDP-α-MSH in the presence of 1 mM $CaCl_2$. The effects of salts with and without 1 nM NDP-α-MSH (a and b) were normalized to the 100 μM Forskolin signal. The concentration-response curves of NDP-α-MSH in the presence of $ZnSO_4$ (c) and $CuCl_2$ (d) were normalized to the NDP-α-MSH signal in the absence of these ions. The data points shown are from a representative experiment of three independent experiments (n = 3) performed in triplicate

the NDP-α-MSH dose–response curves, whereas higher concentrations of Cu^{2+} (>8 μM) caused a downward shift of the curve, which reached even below the baseline (Figure 5d). Also in the case of Cu^{2+}, no substantial changes in the potency of the ligand were observed in the presence of the ion at concentrations up to 16 μM.

3.6.4 | The effect of Zn^{2+} and Cu^{2+} ions on ligand-induced partial agonism

We used HS024, which is known as an antagonist of the MC_4R, to inhibit the activation of receptors by agonists and metal ions. In the cells with MC_4R, HS024 caused a concentration-dependent inhibition of the NDP-α-MSH-induced cAMP accumulation (Figure 6a, diamonds). As HS024 behaved as a partial agonist in our system, the inhibition was not down to the bottom but remained on the level induced by HS024 (Figure 6a, circles). The pIC_{50} value for HS024 in competition with 1 nM NDP-α-MSH was 8.4 ± 0.5. The inhibitory effect of HS024 could also be determined if the accumulation of cAMP was induced by 3 μM Zn^{2+}, but in this case, the pIC_{50} of the ligand was 6.3 ± 0.2 (Figure 6a, triangles). The situation with 3 μM Cu^{2+} was quite different as the ion induced the same level of cAMP accumulation as HS024 alone. Using these reagents together caused a slight increase over the level of the maximal response of HS024 (Figure 6a, squares). A similar effect was also observed if Cu^{2+} was incubated together with the full agonist NDP-α-MSH (Figure 5d, squares).

Classical Schild analysis (Schild, 1949) has often been used to determine competitive mechanisms between agonists and antagonists. In our assay system, HS024 acted as a competitive inhibitor of the response of the full agonist NDP-α-MSH, causing a concentration-dependent rightward shift of the dose–response curves without affecting the level of the maximal signal (Figure 6b). The situation was more complex with Zn^{2+}, where HS024 induced a concentration-dependent rightward shift of the dose–response curves but also reduced the maximal signal of Zn^{2+} ions at higher HS024 concentrations (>3 μM) (Figure 6c). The biphasic dose–response curve of Cu^{2+} was also affected by HS024 (Figure 6d). There was no concentration-dependent shift of the curve, whereas in the presence of HS024, the inhibitory effect of Cu^{2+} disappeared. In the case of NDP-α-MSH, the slope of the Schild-plot was 1.11 ± 0.14, and the pA_2 value of HS024 was 9.8 ± 0.2 (Figure 6e, circles), which is in agreement with the pEC_{50} value determined from HS024 direct activation of cAMP production (Figure 4). The slope close to unity and the observation that HS024 did not affect the maximal signal of NDP-α-MSH (Figure 6b) indicated that they were competitive ligands. In the case of Zn^{2+}, the Schild plot was not linear and reached a plateau at higher HS024 concentrations (from 1 μM) (Figure 6e, triangles). The slope of the linear part of the Schild plot was 0.63 ± 0.05, and the estimated pA_2 value from this part for HS024 was 7.9 ± 0.3 (Figure 6e, triangles). These results indicated that inhibition of the Zn^{2+} ion effect by HS024 did not occur in a competitive manner and that the ion affects via an allosteric site of the MC_4R. In the case of Cu^{2+}, the classical Schild-plot could not be generated. Nevertheless,

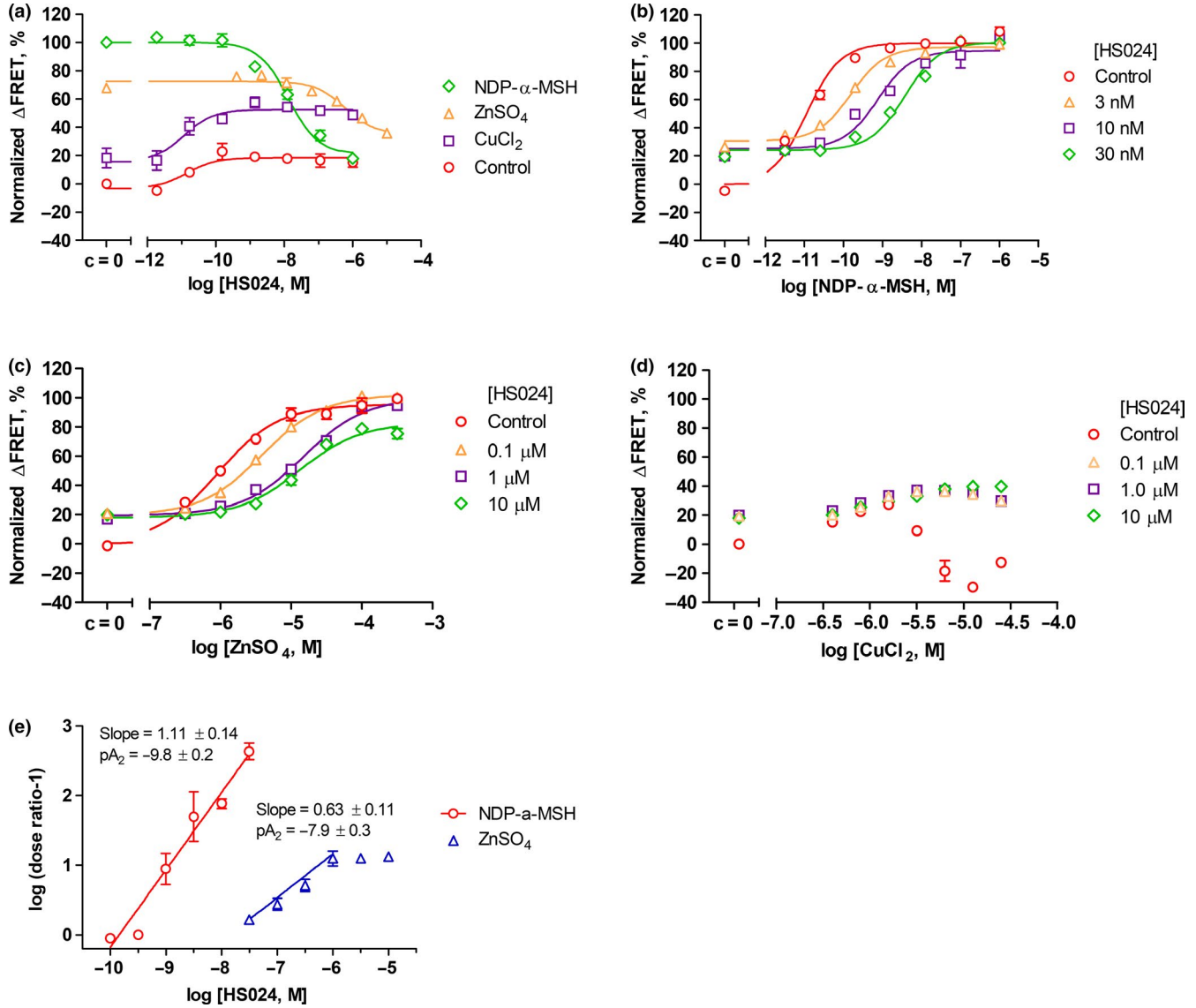

FIGURE 6 Influence of HS024 on the NDP-α-MSH, $ZnSO_4$, and $CuCl_2$-induced production of cAMP in CHO-K1-MC_4R cells. (a): Concentration-dependent influence of HS024 on the cAMP level in the absence or presence of 1 nM NDP-α-MSH, 3 μM $ZnSO_4$, or 3 μM $CuCl_2$. Influence of different concentrations of HS024 on the concentration–response curves of NDP-α-MSH (b), $ZnSO_4$ (c), and $CuCl_2$ (d). The cAMP level was measured as ΔFRET values of CHO-K1-MC_4R cells expressing the cAMP biosensors BacMam-$Epac^{H187}$ 30 min after addition of ligands and/or modulators ($ZnSO_4$ or $CuCl_2$) in the presence of 1 mM $CaCl_2$. The concentration–response graphs show data points from a representative experiment of at least three independent experiments ($n \geq 3$) performed in triplicate and normalized to the maximal NDP-α-MSH signal. (e) Schild plots of HS024 in inhibition of responses of NDP-α-MSH and $ZnSO_4$. Data points are from at least four independent experiments ($n \geq 4$) performed in triplicate and are shown as the mean ± *SD*

the blocking effect of HS024 on Cu^{2+}-induced inhibitory response (Figure 6d) confirmed the assumption that the decrease in cAMP levels generated by these ions in CHO-K1-MC_4R cells (Figure 5a, circles) was because of the interaction with the receptor.

4 | DISCUSSION

It is known that different metal ions may play an important role in the signal transduction of GPCRs. In our study, the complex role of metal ions became evident when fluorescent ligand binding to MC_4R in the presence of 1 mM Ca^{2+} almost doubled in the presence of a small concentration of EDTA. This result indicated that the samples could contain some metal ions, which inhibited ligand binding to MC_4R but could be chelated with EDTA. Ca^{2+} was ruled out, as these ions are essential for high-affinity ligand binding to MC_4R (Kopanchuk *et al.*, 2005; Veiksina *et al.*, 2010). Additionally, the amount of added EDTA was substantially lower than the amount of Ca^{2+} in the reaction medium. If EDTA was added to the medium without Ca^{2+}, there was no specific ligand binding to MC_4R (Figure 1a). ICP-MS analysis revealed that the preparation of BBVs displaying MC_4R contained in addition to calcium and the prescribed buffer components (sodium

and potassium), a significant amount of magnesium, manganese, zinc, and copper (Figure 1c). The source of these metal residues were likely either the Sf9 cells or its growth medium and were trapped during the production of BBV. Mg^{2+}, Mn^{2+}, Zn^{2+}, and Cu^{2+} are abundant functionally essential ions in the human body and have been shown to modulate the ligand binding of several GPCRs (Westhuizen *et al*., 2015), including melanocortin receptors (Holst *et al*., 2002; Lagerström *et al*., 2003; Kopanchuk *et al*., 2005; Mazina *et al*., 2012). Therefore, we studied the potential inhibitory effect of these ions toward ligand binding to MC_4R, which was performed in the presence of at least millimolar concentration of Ca^{2+}, required for high-affinity ligand binding (Kopanchuk *et al*., 2005).

It was shown that Mg^{2+} and Mn^{2+} had no essential effect on ligand binding to the MC_4R in either the presence or absence of Ca^{2+} (Figure 1, d and e). These ions are mainly known to influence the high-affinity agonist binding through indirect effect as it enables the formation of nucleotide-free G-protein complex with the receptor. Our system, however, does not exclude an indirect influence of Mg^{2+} and Mn^{2+} on the ligand binding to MC_4R, as G proteins are not co-expressed in BBV (Wenzel-Seifert and Seifert, 2000; Uustare, Näsman, Åkerman, and Rinken, 2004; Tõntson, Kopanchuk, and Rinken, 2014).

Conversely, Zn^{2+} and Cu^{2+} had a substantial inhibitory effect on the ligand binding to MC_4R even at low micromolar concentrations. To understand the modulation mechanisms of these ions, different probes of MC_4R were used in this study: TAMRA-NDP-α-MSH exhibits full agonistic properties, whereas Cy3B-labeled UTBC102 is a partial agonist and UTBC101 has minimal agonistic activity. From the perspective of kinetic studies, UTBC101 and TAMRA-NDP-α-MSH have very slow dissociation kinetics, whereas the lower affinity of UTBC102 is compensated by its faster kinetics (Veiksina *et al*., 2010; Link *et al*., 2017). For all the ligands, Zn^{2+} and Cu^{2+} caused a concentration-dependent and complete inhibition of the binding to MC_4R. The inhibitory effect of these ions on the ligand binding to MC_4R has been found also in earlier studies (Holst *et al*., 2002; Lagerström *et al*., 2003). However, in these systems even millimolar Zn^{2+} concentrations did not cause full inhibition ^{125}I-NDP-α-MSH binding (Holst *et al*., 2002). It is important to mention that already submillimolar concentrations of zinc and copper have a substantial effect on the level of non-specific binding of ligands. These ions form insoluble aggregates already at submillimolar concentrations, depending on the pH as well as on the buffer composition (Ferreira *et al*. 2015; Krężel and Maret, 2016). In our study, the concentrations of Zn^{2+} and Cu^{2+} used remained in most cases in the low micromolar range, in which case the proportion of insoluble aggregates is low and has a modest effect on the level of non-specific binding. Nevertheless, we measured the non-specific binding in all the experiments and took into account for the determination of the specific ligand-binding level.

The concentrations of Zn^{2+} and Cu^{2+}, which caused 50% inhibition of the ligand binding to MC_4R (IC_{50}), depended on the nature of the fluorescent ligand used. Zn^{2+} was more efficient at inhibiting the binding of the UTBC102 compared to UTBC101. For Cu^{2+}, the opposite was observed. In the earlier study, Zn^{2+} also showed a higher potency than Cu^{2+} upon inhibition of ^{125}I-NDP-α-MSH binding to MC_4R (Holst *et al*., 2002). It is not uncommon that the effects of allosteric modulators vary depending on the nature of the orthosteric GPCR ligand (Kenakin, 2005a), which was probably the case herein.

Monitoring of the binding kinetics of different MC_4R fluorescent ligands revealed that Zn^{2+} and Cu^{2+} both inhibited the formation of receptor-ligand complexes and initiated the dissociation of the already formed complexes. Furthermore, the rate of dissociation depended on the concentration of the ions. For example, the dissociation of UTBC101 could already be initiated with 1 μM Zn^{2+}, which was accelerated up to 20-fold with the increase in the ion concentration up to 32 μM. This finding indicates that the ions do not compete with the ligands for the orthosteric-binding site, but instead have a negative allosteric effect on ligand binding (May *et al*., 2007). The concentration-dependent acceleration of dissociation was also induced by Cu^{2+}, but in a more complex manner, as the kinetics did not correspond to a simple one-phase decay. Here, the interpretation of dissociation kinetics could also be complicated by the quenching effect of Cu^{2+} on the fluorescent intensities of ligands, which appeared at higher micromolar concentrations. It was complicated to entirely separate the changes in FA values caused by the dissociation of the ligand and the quenching of the fluorophore. However, it is clear that the determined inhibitory effect of Cu^{2+} on ligand binding was not an apparent effect of the quenching, as the inhibition already appeared at such low ion concentrations, where there was no detectable quenching of the fluorescent intensity. The role of Zn^{2+} as an allosteric modulator has also been found in the case of D_1, D_{2L}, and D_3 dopamine receptors, where it accelerates antagonist dissociation (Schetz and Sibley, 1997; Schetz, Chu, and Sibley, 1999), as well as in the case of β_2- and α_{1A}-adrenoreceptors, where it slows down the dissociation (Swaminath, Lee, and Kobilka, 2003; Ciolek, Maïga, Marcon, Servent, and Gilles, 2011). The role of Cu^{2+} as an allosteric modulator has been found in the case of α_{1A}-adrenoreceptors, although it does not influence ligand dissociation rates (Ciolek *et al*., 2011). To our knowledge, there are no earlier reports in which the negative allosteric effect of Zn^{2+} and Cu^{2+} have been demonstrated to alter the dissociation kinetics of ligands from MC_4R.

The inhibitory effect of Zn^{2+} on ligand binding could be readily reversed with excess EDTA but only in the case of low micromolar Zn^{2+} concentrations. In the case of higher ion concentrations, some loss of binding occurred. In contrast, full restoration of binding could not be achieved at any of the studied Cu^{2+} concentrations. Therefore, the presence of relatively low concentrations of these ions in assay buffers may irreversibly inhibit ligand binding to MC_4R. The reversibility of the inhibitory effects of Zn^{2+} and Cu^{2+} by EDTA has also been found in studies of α_{1A}-adrenoreceptors and different dopamine receptor subtypes (Schetz and Sibley, 1997; Schetz *et al*., 1999; Ciolek *et al*., 2011).

The influence of Zn^{2+} and Cu^{2+} on the signal transduction of MC_4R was studied in stable CHO-K1 cells expressing MC_4R by measuring the cAMP level with $Epac^{H187}$ biosensors. Zn^{2+} by itself caused a concentration-dependent accumulation of cAMP and acted as a practically full agonist of MC_4R with an EC_{50} value of 1.1 μM. In

the brain, free (rapidly exchangeable) zinc is mostly sequestered in the pre-synaptic vesicles of glutamatergic nerve terminals, and upon stimulation, these zinc-releasing neurons also release glutamate into the synaptic cleft (Minami, Takeda, Yamaide, and Oku, 2002; Takeda, Minami, Seki, Nakajima, and Oku, 2004). Upon stimulation, the free concentration of synaptically released zinc has been found to reach the 10–30 μM range on average in brain slices (Thompson, Whetsell, Maliwal, Fierke, and Frederickson, 2000; Li, Hough, Frederickson, and Sarvey, 2001a; Li, Hough, Suh, Sarvey, and Frederickson, 2001b; Ueno *et al*., 2002). As ligand binding to MC_4R was already modulated by a low micromolar concentration of Zn^{2+}, these ions may play a physiologically relevant role in the activation of these receptors. For example, the glutamatergic system has been found to be connected with MC_4R function of body weight regulation in the hypothalamus (Xu *et al*., 2013). Intriguingly, we observed that Cu^{2+} ions induced a biphasic cellular response, increasing the cAMP accumulation at ion concentrations up to 1.5 μM, but at higher concentrations decreasing it to below the basal response level. Here, we propose that only suppression of the basal response by Cu^{2+} ions is likely mediated through MC_4R, as this kind of decrease in the cAMP accumulation was not observed in the naive CHO-K1 cells without MC_4R. It is known that Cu^{2+} ions are also essential for proper functioning of the CNS, but their metabolism is very tightly controlled (D'Ambrosi and Rossi, 2015). However, these ions may function as endogenous inverse agonists for MC_4R. Earlier studies have described that Zn^{2+} may function as a partial agonist or as an antagonist, whereas for Cu^{2+} there are no reports on its function for MC_4R (Holst *et al*., 2002; Lagerström *et al*., 2003). A critical issue in these assays is the basal concentration of the ions, which may cause very different results in the case of such an ion-sensitive system (Ferreira *et al*. 2015; Krężel and Maret, 2016).

Among other GPCRs, MC_4Rs have been found to exhibit relatively high constitutive activity in vitro in the absence of agonistic ligands (Haskell-Luevano and Monck, 2001; Nijenhuis *et al*., 2001; Coll, 2013). Although the nature of constitutive activity has been described as spontaneous, its mechanism is not yet fully understood. Zn^{2+} is often used as a required nutrient in cell culture medium, and its total concentration in cells may in some cases reach as high as 100 μM (Bozym *et al*., 2008). Even if most of the Zn^{2+} from the medium is bound to different proteins, there is an equilibrium between bound and free Zn^{2+}. Therefore, Zn^{2+} may be the reason for the described increased basal activity of MC_4R in cAMP pathway. As it has been shown that Zn^{2+} induces agonistic signal also for of MC_1R, G-protein-coupled receptors 83 and 93, the presence of Zn^{2+} could be the reason for the higher constitutive activity of these GPCRs (Holst *et al*., 2002, 2004; Müller *et al*., 2013). Cu^{2+} may be another key player, but in an opposite manner, as it reduces the basal activity of MC_4R in cAMP pathway. Copper is also an essential element in cell cultures, and its content in the medium (0.8–2.3 μM) is generally achieved by the addition of 10% serum, although in some cases additional copper salts may also be used (Chaderjian, Chin, Harris, and Etcheverry, 2005; Qian *et al*., 2011). Thus, the interplay between zinc and copper ions may have a crucial impact on the determination of the responsiveness of MC_4R in cAMP pathway, as Zn^{2+} behaves as an agonist and Cu^{2+} as an inverse agonist.

Of course, the definition of ligand function is not absolute as their behavior also depends on the level of basal activity of receptors (Kenakin, 2005b; Bond and IJzerman 2006). Elevated basal activity is usually required to define the inverse agonistic properties of ligands. This is also the case for MC_4R, where the endogenous antagonist agouti-related protein (Ollmann *et al*., 1997) has been demonstrated to act as an inverse agonist for these receptors with elevated basal activity in cAMP pathway (Haskell-Luevano and Monck, 2001; Nijenhuis *et al*., 2001). On the contrary, the tetrapeptide His-DNal(2′)-Arg-Trp have found to act as an antagonist (Holder, Bauzo, Xiang, and Haskell-Luevano, 2002; Chen, Georgeson, Harmon, Haskell-Luevano, and Yang, 2006), but also as a partial agonist in cAMP pathway for MC_4R (Lensing *et al*., 2019). Similarly, in this study, HS024 exhibited minimal agonist activity of MC_4R in cAMP pathway, despite being previously reported as an antagonist of this receptor (Kask *et al*., 1998). In relation to the currently determined function of HS024, Zn^{2+} and Cu^{2+} ions clearly behaved as agonists and inverse agonists, respectively.

As we determined that Zn^{2+} and Cu^{2+} ions modulate the basal activity of MC_4R, the question was how these ions modulate the signal transduction of orthosteric ligands. The addition of Zn^{2+} ions together with the full agonist NDP-α-MSH caused a concentration-dependent increase in the basal level of the ligand dose–response curve without affecting its potency. However, the addition of Cu^{2+} at concentrations above 4 μM caused a decrease in the basal level of the ligand dose–response curve without substantially affecting its potency. These data confirm that these ions do not compete with ligands for binding to the orthosteric site, while they function via an allosteric site. It is important to point out that both metal ions also slightly enhanced the maximal cAMP response level of the full agonist NDP-α-MSH. However, a similar modest ion-induced increase in the cAMP level was also found after blocking the receptors with HS024 and in the naive CHO-K1 cells without MC_4R. Thus, it can be proposed that the ion-induced increase in the maximal level of cAMP is not associated with the direct activation of MC_4R.

The allosteric nature of Zn^{2+} was also observed if its agonistic properties were inhibited with HS024. In the case of the full agonist NDP-α-MSH, HS024 effectively inhibited its agonistic response, and the slope of the Schild plot was close to unity, which indicates that these ligands compete for the orthosteric site of MC_4R. In the case of Zn^{2+}, the HS024 could also inhibit the response, but it was considerably less effective, and the slope of the Schild plot was substantially less than one. This finding indicates that HS024 is not a competitive inhibitor of Zn^{2+} and confirms once again that Zn^{2+} affects MC_4R via an allosteric-binding site. As Cu^{2+} has biphasic response cAMP response, the classical Schild analysis could not be used to study its mode of action, but HS024 could be used to block the inverse agonistic response of the copper ions in a concentration-dependent manner. This result once again confirms that Cu^{2+} ions indeed modulate the signal transduction of MC_4R. It is important to mention, that all these studies were directed to the activation

of cAMP signaling pathway, but it is known that MC_4R can activate also other G proteins and ERK1/2 pathway (Yang and Tao, 2017), but how these ions affect these systems remains for the further studies.

Thus, we have shown that Zn^{2+} and Cu^{2+} are allosteric modulators of the ligand binding and signal transduction of MC_4R at physiologically relevant low micromolar concentrations. Zn^{2+} ions have clear agonistic properties toward MC_4R, whereas Cu^{2+} ions function as inverse agonists. As zinc is abundantly found in the CNS, these ions may have a crucial role in the regulation of signaling in the melanocortin system. Although the level of free copper in the CNS is more strictly controlled, its inverse agonistic role in the melanocortin system may also have physiological relevance. Importantly, Zn^{2+} and Cu^{2+} are also commonly found in cell culture media, where their free concentration is not clearly defined and may have a direct influence on experimental results concerning MC_4Rs.

ACKNOWLEDGMENTS

This work the by the Estonian Research Council grants (IUT20-17 and PSG230). We thank Dr. Olga Mazina for help with construction of the baculoviruses carrying the recombinant gene encoding the cAMP biosensor.

CONFLICT OF INTEREST

The authors declare that they have no conflicts of interest with the contents of this article.

All experiments were conducted in compliance with the ARRIVE guidelines.

OPEN SCIENCE BADGES

This article has received a badge for *__Open Materials__* because it provided all relevant information to reproduce the study in the manuscript. More information about the Open Science badges can be found at https://cos.io/our-services/open-science-badges/.

ORCID

Santa Veiksina https://orcid.org/0000-0003-4191-4354
Maris-Johanna Tahk https://orcid.org/0000-0002-4566-9192
Tõnis Laasfeld https://orcid.org/0000-0002-4730-3047
Sergei Kopanchuk https://orcid.org/0000-0003-1756-9327
Ago Rinken https://orcid.org/0000-0002-7238-749X

REFERENCES

Biebermann, H., Krude, H., Elsner, A., Chubanov, V., Gudermann, T., & Grüters, A. (2003). Autosomal-dominant mode of inheritance of a melanocortin-4 receptor mutation in a patient with severe early-onset obesity is due to a dominant-negative effect caused by receptor dimerization. *Diabetes*, *52*, 2984–2988. https://doi.org/10.2337/diabetes.52.12.2984

Bitanihirwe, B.K.Y., & Cunningham, M.G. (2009). Zinc: The brain's dark horse. *Synapse*, *63*, 1029–1049. https://doi.org/10.1002/syn.20683

Bond, R.A., & IJzerman A.P. (2006). Recent developments in constitutive receptor activity and inverse agonism, and their potential for GPCR drug discovery. *Trends Pharmacol. Sci.*, *27*, 92–96.

Bozym, R., Hurst, T.K., Westerberg, N., Stoddard, A., Fierke, C.A., Frederickson, C.J., & Thompson, R.B. (2008). *Chapter 14 Determination of zinc using carbonic anhydrase-based fluorescence biosensors*, in Methods in Enzymology, Vol. *450* (pp. 287–309). Academic Press.

Chaderjian, W.B., Chin, E.T., Harris, R.J., & Etcheverry, T.M. (2005). Effect of copper sulfate on performance of a serum-free CHO cell culture process and the level of free thiol in the recombinant antibody expressed. *Biotechn. Progr.*, *21*, 550–553. https://doi.org/10.1021/bp0497029

Chapman, K.L., & Findlay, J.B.C. (2013). The melanocortin 4 receptor: Oligomer formation, interaction sites and functional significance. *Biochim. Biophys. Acta - Biomembranes*, *1828*, 535–542. https://doi.org/10.1016/j.bbamem.2012.10.011

Chen, M., Georgeson, K.E., Harmon, C.M., Haskell-Luevano, C., & Yang, Y. (2006). Functional characterization of the modified melanocortin peptides responsible for ligand selectivity at the human melanocortin receptors. *Peptides*, *27*, 2836–2845. https://doi.org/10.1016/j.peptides.2006.04.012

Ciolek, J., Maïga, A., Marcon, E., Servent, D., & Gilles, N. (2011). Pharmacological characterization of zinc and copper interaction with the human alpha1A-adrenoceptor. *Eur. J. Pharmacol.*, *655*, 1–8.

Coll, A.P. (2013). Are melanocortin receptors constitutively active in vivo? *Eur. J. Pharmacol.*, *719*, 202–207. https://doi.org/10.1016/j.ejphar.2013.04.051

D'Ambrosi, N., & Rossi, L. (2015). Copper at synapse: Release, binding and modulation of neurotransmission. *Neurochem. Int.*, *90*, 36–45. https://doi.org/10.1016/j.neuint.2015.07.006

Elsner, A., Tarnow, P., Schaefer, M., Ambrugger, P., Krude, H., Grüters, A., & Biebermann, H. (2006). MC4R oligomerizes independently of extracellular cysteine residues. *Peptides*, *27*, 372–379. https://doi.org/10.1016/j.peptides.2005.02.027

Ericson, M.D., Lensing, C.J., Fleming, K.A., Schlasner, K.N., Doering, S.R., & Haskell-Luevano, C. (2017). Bench-top to clinical therapies: A review of melanocortin ligands from 1954 to 2016. *Biochimica et Biophysica Acta - Molecular Basis of Disease*, *1863*, 2414–2435.

Ferreira, C.M.H., Pinto, I.S.S., Soares, E.V., & Soares, H.M.V.M. (2015). (Un)suitability of the use of pH buffers in biological, biochemical and environmental studies and their interaction with metal ions – a review. *RSC Advances*, *5*, 30989–31003. https://doi.org/10.1039/C4RA15453C

Haskell-Luevano, C., & Monck, E.K. (2001). Agouti-related protein functions as an inverse agonist at a constitutively active brain melanocortin-4 receptor. *Regul. Peptides*, *99*, 1–7. https://doi.org/10.1016/S0167-0115(01)00234-8

Haskell-Luevano, C., Hendrata, S., North, C., Sawyer, T.K., Hadley, M.E., Hruby, V.J., … Gantz, I. (1997). Discovery of prototype peptidomimetic agonists at the human melanocortin receptors MC1R and MC4R. *J. Med. Chem.*, *40*, 2133–2139.

Hoffmann, C., Castro, M., Rinken, A., Leurs, R., Hill, S.J., & Vischer, H.F. (2015). Ligand residence time at G-protein–coupled receptors—why we should take our time to study it. *Mol. Pharmacol.*, *88*, 552–560.

Holder, J.R., Bauzo, R.M., Xiang, Z., & Haskell-Luevano, C. (2002). Structure–activity relationships of the melanocortin tetrapeptide Ac-His-DPhe-Arg-Trp-NH_2 at the mouse melanocortin receptors: Part 2 modifications at the Phe position. *J. Med. Chem.*, *45*, 3073–3081.

Holst, B., Elling, C.E., & Schwartz, T.W. (2002). Metal ion-mediated agonism and agonist enhancement in melanocortin MC1 and MC4 receptors. *J. Biol. Chem.*, *277*, 47662–47670.

Holst, B., Holliday, N.D., Bach, A., Elling, C.E., Cox, H.M., & Schwartz, T.W. (2004). Common structural basis for constitutive activity of the ghrelin receptor family. *J. Biol. Chem.*, *279*, 53806–53817.

Kask, A., Mutulis, F., Muceniece, R., Pähkla, R., Mutule, I., Wikberg, J.E.S., … Schiöth, H.B. (1998). Discovery of a novel superpotent and

selective melanocortin-4 receptor antagonist (HS024): Evaluation in vitro and in vivo. *Endocrinology*, *139*, 5006–5014.

Kenakin, T. (2005a). New concepts in drug discovery: Collateral efficacy and permissive antagonism. *Nat. Rev. Drug Discovery*, *4*, 919. https://doi.org/10.1038/nrd1875

Kenakin, T. (2005b). The physiological significance of constitutive receptor activity. *Trends Pharmacol. Sci.*, *26*, 603–605. https://doi.org/10.1016/j.tips.2005.10.007

Klarenbeek, J., Goedhart, J., van Batenburg, A., Groenewald, D., & Jalink, K. (2015). Fourth-generation Epac-based FRET sensors for cAMP feature exceptional brightness, photostability and dynamic range: Characterization of dedicated sensors for FLIM, for ratiometry and with high affinity. *PLoS ONE*, *10*, e0122513. https://doi.org/10.1371/journal.pone.0122513

Kopanchuk, S., Veiksina, S., Petrovska, R., Mutule, I., Szardenings, M., Rinken, A., & Wikberg, J.E.S. (2005). Co-operative regulation of ligand binding to melanocortin receptor subtypes: Evidence for interacting binding sites. *Eur. J. Pharmacol.*, *512*, 85–95. https://doi.org/10.1016/j.ejphar.2005.02.021

Kopanchuk, S., Veiksina, S., Mutulis, F., Mutule, I., Yahorava, S., Mandrika, I., … Wikberg, J.E.S. (2006). Kinetic evidence for tandemly arranged ligand binding sites in melanocortin 4 receptor complexes. *Neurochem. Int.*, *49*, 533–542.

Krężel, A., & Maret, W. (2016). The biological inorganic chemistry of zinc ions. *Arch. Biochem. Biophys.*, *611*, 3–19.

Laasfeld, T., Kopanchuk, S., & Rinken, A. (2017). Image-based cell-size estimation for baculovirus quantification. *Biotechniques*, *63*, 161–168. https://doi.org/10.2144/000114595

Lagerström, M.C., Klovins, J., Fredriksson, R., Fridmanis, D., Haitina, T., Ling, M.K., … Schiöth, H.B. (2003). High affinity agonistic metal ion binding sites within the melanocortin 4 receptor illustrate conformational change of transmembrane region 3. *J. Biol. Chem.*, *278*, 51521–51526.

Lensing, C.J., Freeman, K.T., Schnell, S.M., Speth, R.C., Zarth, A.T., & Haskell-Luevano, C. (2019). Developing a biased unmatched bivalent ligand (BUmBL) design strategy to target the GPCR homodimer allosteric signaling (cAMP over β-arrestin 2 recruitment) within the melanocortin receptors. *J. Med. Chem.*, *62*, 144–158.

Li, Y., Hough, C.J., Frederickson, C.J., & Sarvey, J.M. (2001a). Induction of mossy Fiber→Ca3 long-term potentiation requires translocation of synaptically released Zn^{2+}. *J. Neurosci.*, *21*, 8015–8025.

Li, Y., Hough, C.J., Suh, S.W., Sarvey, J.M., & Frederickson, C.J. (2001b). Rapid translocation of Zn2+ from presynaptic terminals into postsynaptic hippocampal neurons after physiological stimulation. *J. Neurophysiol.*, *86*, 2597–2604.

Link, R., Veiksina, S., Rinken, A., & Kopanchuk, S. (2017). Characterization of ligand binding to melanocortin 4 receptors using fluorescent peptides with improved kinetic properties. *Eur. J. Pharmacol.*, *799*, 58–66.

May, L.T., Leach, K., Sexton, P.M., & Christopoulos, A. (2007). Allosteric modulation of G protein–coupled receptors. *Annu. Rev. Pharmacol. Toxicol.*, *47*, 1–51.

Mazina, O., Reinart-Okugbeni, R., Kopanchuk, S., & Rinken, A. (2012). BacMam system for FRET-based cAMP sensor expression in studies of melanocortin MC1 receptor activation. *J. Biomol. Screen.*, *17*, 1096–1101.

Mazina, O., Allikalt, A., Heinloo, A., Reinart-Okugbeni, R., Kopanchuk, S., & Rinken, A. (2015a). cAMP assay for GPCR ligand characterization: Application of BacMam expression system. In D.M.F. Prazeres & S.A.M. Martins (Eds.), *G protein-coupled receptor screening assays: Methods and protocols* (pp. 65–77). New York, NY: Springer.

Mazina, O., Luik, T., Kopanchuk, S., Salumets, A., & Rinken, A. (2015b). Characterization of the biological activities of human luteinizing hormone and chorionic gonadotropin by a Förster resonance energy transfer-based biosensor assay. *Anal. Lett.*, *48*, 2799–2809. https://doi.org/10.1080/00032719.2015.1052140

Minami, A., Takeda, A., Yamaide, R., & Oku, N. (2002). Relationship between zinc and neurotransmitters released into the amygdalar extracellular space. *Brain Res.*, *936*, 91–94. https://doi.org/10.1016/S0006-8993(02)02499-X

Müller, A., Kleinau, G., Piechowski, C.L., Müller, T.D., Finan, B., Pratzka, J., … Biebermann, H. (2013). G-protein coupled receptor 83 (GPR83) signaling determined by constitutive and zinc(II)-induced activity. *PLoS ONE*, *8*, e53347. https://doi.org/10.1371/journal.pone.0053347

Müller, A., Berkmann, J.C., Scheerer, P., Biebermann, H., & Kleinau, G. (2016). Insights into basal signaling regulation, oligomerization, and structural organization of the human G-protein coupled receptor 83. *PLoS ONE*, *11*, e0168260. https://doi.org/10.1371/journal.pone.0168260

Nickolls, S.A., & Maki, R.A. (2006). Dimerization of the melanocortin 4 receptor: A study using bioluminescence resonance energy transfer. *Peptides*, *27*, 380–387. https://doi.org/10.1016/j.peptides.2004.12.037

Nijenhuis, W.A.J., Oosterom, J., & Adan, R.A.H. (2001). AgRP(83–132) acts as an inverse agonist on the human-melanocortin-4 receptor. *Mol. Endocrinol.*, *15*, 164–171.

Ollmann, M.M., Wilson, B.D., Yang, Y.-K., Kerns, J.A., Chen, Y., Gantz, I., & Barsh, G.S. (1997). Antagonism of central melanocortin receptors in vitro and in vivo by agouti-related protein. *Science*, *278*, 135–138. https://doi.org/10.1126/science.278.5335.135

Qian, Y., Khattak, S.F., Xing, Z., He, A., Kayne, P.S., Qian, N.-X., … Li, Z.J. (2011). Cell culture and gene transcription effects of copper sulfate on Chinese hamster ovary cells. *Biotechnol. Progress*, *27*, 1190–1194.

Rediger, A., Tarnow, P., Bickenbach, A., Schaefer, M., Krude, H., Grüters, A., & Biebermann, H. (2009). Heterodimerization of hypothalamic G-protein-coupled receptors involved in weight regulation. *OFA*, *2*, 80–86. https://doi.org/10.1159/000209862

Rinken, A., Lavogina, D., & Kopanchuk, S. (2018). Assays with detection of fluorescence anisotropy: Challenges and possibilities for characterizing ligand binding to GPCRs. *Trends Pharmacol. Sci.*, *39*, 187–199.

Schetz, J.A., & Sibley, D.R. (1997). Zinc allosterically modulates antagonist binding to cloned D1 and D2 dopamine receptors. *J. Neurochem.*, *68*, 1990–1997. https://doi.org/10.1046/j.1471-4159.1997.68051990.x

Schetz, J.A., Chu, A., & Sibley, D.R. (1999). Zinc modulates antagonist interactions with D2-like dopamine receptors through distinct molecular mechanisms. *J. Pharmacol. Exp. Ther.*, *289*, 956–964.

Schild, H.O. (1949). pAx and competitive drug antagonism. *British Journal of Pharmacology and Chemotherapy*, *4*, 277–280.

Swaminath, G., Lee, T.W., & Kobilka, B. (2003). Identification of an allosteric binding site for Zn2+ on the β2 adrenergic receptor. *J. Biol. Chem.*, *278*, 352–356.

Takeda, A., Minami, A., Seki, Y., Nakajima, S., & Oku, N. (2004). Release of amino acids by zinc in the hippocampus. *Brain Res. Bull.*, *63*, 253–257.

Tao, Y.-X. (2010). The melanocortin-4 receptor: Physiology, pharmacology, and pathophysiology. *Endocr. Rev.*, *31*, 506–543.

Tao, Y.-X. (2014). Constitutive activity in melanocortin-4 receptor: Biased signaling of inverse agonists. *Adv. Pharmacol.*, *70*, 135–154. https://doi.org/10.1016/B978-0-12-417197-8.00005-5

Thompson, R.B., Whetsell, W.O. Jr, Maliwal, B.P., Fierke, C.A., & Frederickson, C.J. (2000). Fluorescence microscopy of stimulated Zn(II) release from organotypic cultures of mammalian hippocampus using a carbonic anhydrase-based biosensor system. *J. Neurosci. Methods*, *96*, 35–45. https://doi.org/10.1016/S0165-0270(99)00183-1

Tõntson, L., Kopanchuk, S., & Rinken, A. (2014). Characterization of 5-HT1A receptors and their complexes with G-proteins in budded baculovirus particles using fluorescence anisotropy of Bodipy-FL-NAN-190. *Neurochem. Int.*, *67*, 32–38. https://doi.org/10.1016/j.neuint.2014.01.012

Ueno, S., Tsukamoto, M., Hirano, T., Kikuchi, K., Yamada, M.K., Nishiyama, N., … Ikegaya, Y. (2002). Mossy fiber Zn^{2+} spillover modulates heterosynaptic N-methyl-d-aspartate receptor activity in hippocampal CA3 circuits. *J. Cell Biol.*, *158*, 215–220.

van Unen, J., Woolard, J., Rinken, A., Hoffmann, C., Hill, S.J., Goedhart, J., … Adjobo-Hermans, M.J.W. (2015). A perspective on studying G-protein–coupled receptor signaling with resonance energy transfer biosensors in living organisms. *Mol. Pharmacol.*, *88*, 589–595.

Uustare, A., Näsman, J., Åkerman, K.E.O., & Rinken, A. (2004). Characterization of M2 muscarinic receptor activation of different G protein subtypes. *Neurochem. Int.*, *44*, 119–124.

Veiksina, S., Kopanchuk, S., & Rinken, A. (2010). Fluorescence anisotropy assay for pharmacological characterization of ligand binding dynamics to melanocortin 4 receptors. *Anal. Biochem.*, *402*, 32–39.

Veiksina, S., Kopanchuk, S., & Rinken, A. (2014). Budded baculoviruses as a tool for a homogeneous fluorescence anisotropy-based assay of ligand binding to G protein-coupled receptors: The case of melanocortin 4 receptors. *Biochimica et Biophysica Acta (BBA) - Biomembranes*, *1838*, 372–381. https://doi.org/10.1016/j.bbamem.2013.09.015

Veiksina, S., Kopanchuk, S., Mazina, O., Link, R., Lille, A., & Rinken, A. (2015). Homogeneous fluorescence anisotropy-based assay for characterization of ligand binding dynamics to GPCRs in budded baculoviruses: The case of Cy3B-NDP-α-MSH binding to MC4 receptors. In D.M.F. Prazeres & S.A.M. Martins (Eds.), *G protein-coupled receptor screening assays: Methods and protocols* (pp. 37–50). New York, NY: Springer.

Wenzel-Seifert, K., & Seifert, R. (2000). Molecular analysis of β2-adrenoceptor coupling to Gs-, Gi-, and Gq-proteins. *Mol. Pharmacol.*, *58*, 954–966.

van der Westhuizen, E.T., Valant, C., Sexton, P.M., & Christopoulos, A. (2015). Endogenous allosteric modulators of G protein–coupled receptors. *J. Pharmacol. Exp. Ther.*, *353*, 246–260.

Wikberg, J.E.S., & Mutulis, F. (2008). Targeting melanocortin receptors: An approach to treat weight disorders and sexual dysfunction. *Nat. Rev. Drug Discovery*, *7*, 307–323. https://doi.org/10.1038/nrd2331

Xu, Y., Wu, Z., Sun, H., Zhu, Y., Kim, E.R., Lowell, B.B., … Tong, Q. (2013). Glutamate mediates the function of melanocortin receptor 4 on Sim1 neurons in body weight regulation. *Cell Metab.*, *18*, 860–870. https://doi.org/10.1016/j.cmet.2013.11.003

Yang, L.-K., & Tao, Y.-X. (2017). Biased signaling at neural melanocortin receptors in regulation of energy homeostasis. *Biochem. Biophys. Acta.*, *1863*, 2486–2495.

SUPPORTING INFORMATION

Additional supporting information may be found online in the Supporting Information section.

How to cite this article: Link R, Veiksina S, Tahk M-J, et al. The constitutive activity of melanocortin-4 receptors in cAMP pathway is allosterically modulated by zinc and copper ions. *J. Neurochem.* 2020;153:346–361. https://doi.org/10.1111/jnc.14933